A DRAG PREDICTION VALIDATION STUDY FOR AIRCRAFT AERODYNAMIC ANALYSIS

Akio OCHI, Eiji SHIMA
Kawasaki Heavy Industries, ltd

Keywords: *CFD, Drag prediction, Validation*

Abstract

A CFD drag prediction validation study was conducted for DLR-F6 aircraft model with wing/body and wing/body/nacelle/pylon configurations. This study was originally conducted for the AIAA Drag Prediction Workshop II (DPW2) at Orland, Florida in Jun. 2003. After the meeting, detailed survey for grid density, turbulence modeling, and transition effects on drag prediction has been performed. As a result, shock wave location is shifted when span-wise direction grid points are increased. Overall agreement between CFD and WTT were fairly good for Wing/Body configuration. Wing/Body/Nacelle/Pylon cases showed rather unsatisfactory agreement. This discrepancy was caused by sensitive separation at inboard side of pylon and wing junction. Lack of grid resolution may cause serious difference of flow separation. Grid convergence could not be obtained through this study.

1 Introduction

For the last decade, Computational Fluid Dynamics (CFD) has become a practical tool of aerodynamic design for aircrafts. However accuracy of CFD drag prediction has not being clear. The accuracy for actual three-dimensional complete aircraft geometry with engine nacelle and pylon is not clear. In addition, CFD results were considerably depended on grid parameters such as grid density, and also grid generation operator. This vagueness has prevented CFD from being used as a principal aerodynamic design tool. To recognize CFD as a principal tool, it must be known how much difference exists between CFD prediction and wind tunnel result, in addition, the grid influence is also be cleared.

2 Grid systems

2.1 Model geometry

The calculated model is the DLR-F6. It is a transport aircraft configuration as shown in Fig.1. The geometry definition data was provided by the AIAA Drag Prediction workshop [1] officials as an IGES (Initial Graphics Exchange Specification) file. There are two types of DLR-F6 used in the workshop. One is a Wing and Body configuration. Another is a Wing/Body/Nacelle/Pylon configuration.

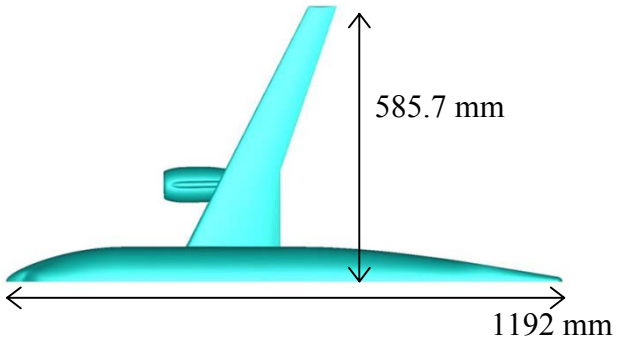

Fig. 1. DLR-F6 geometry with wing/body/ nacelle /pylon configuration.

2.2 Hybrid Grid System

A hybrid unstructured grid system was utilized in this computation. It consists of a large number of hexahedral and prism volume cells and small portion of pyramid and tetra cells. Volume grid cells are piled up from a surface grid as shown in Fig.2. Therefore hexahedral volume cells are produced on quadrilateral surface cells and prism volume cells are produced on triangle surface cells. This grid generation is performed by PUFGG [2] (Pile-Up Forming Grid Generator) developed by the authors.

One of the advantages of PUFGG is that it is capable to generate volume grid from mixed quadrilateral and triangular surface meshes. Hexahedral volume cell has a good property to obtain higher accuracy and higher resolution. In particularly, Quadrilateral surface mesh has a benefit for anisotropic shape such as leading and trailing edge sections on a wing. If all triangles mesh is used, the number of surface grid points should be considerably increased to achieve same resolution and accuracy. On the other hand triangular surface mesh is suitable for automatic surface mesh generation. In the present study, surface meshes were created using commercial software. As shown in Figs. 3 and 4, quadrilateral cells are mainly used in the present study.

During piling up process, grid points will be merged to keep grid spacing as shown Fig. 5. Figure 6 shows an example of grid merging to generate concave region.

Several different directional grid refinements were employed to investigate effect on aerodynamic characteristics. Five grids were generated for WB (Wing/Body) configuration and three grids were generated for WBNP (Wing/Body/Nacelle/Pylon) configuration as shown in Table 1. Span, chord, normal direction refinement was separately applied especially for Wing/Body configuration. Grid generation time is about an hour using Pentium 4 PC for WBNP grid, which has several million volume cells.

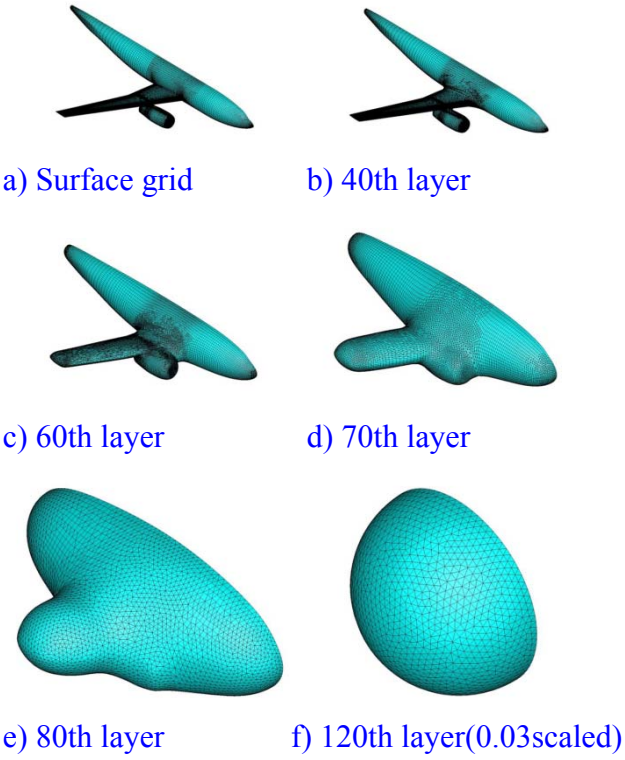

a) Surface grid b) 40th layer

c) 60th layer d) 70th layer

e) 80th layer f) 120th layer(0.03scaled)

Fig. 2. Growing volume grid during grid generation process by PUFGG.

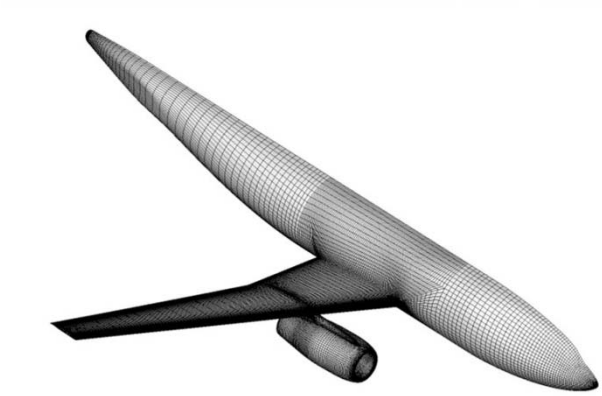

Fig. 3. Surface mesh for DLR-F6 WBNP configuration. (Medium density grid).

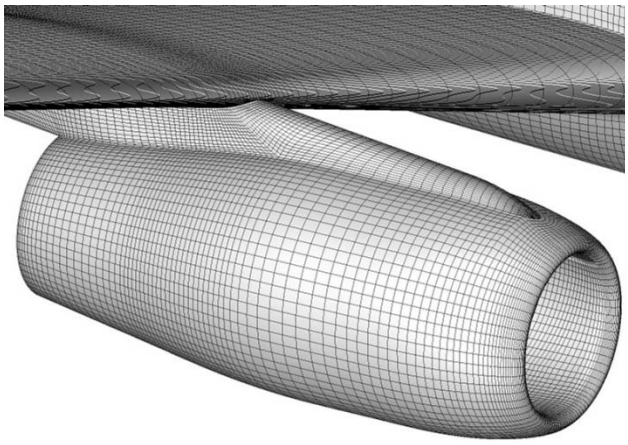

Fig. 4. Surface mesh for DLR-F6 close up around nacelle (Medium density grid).

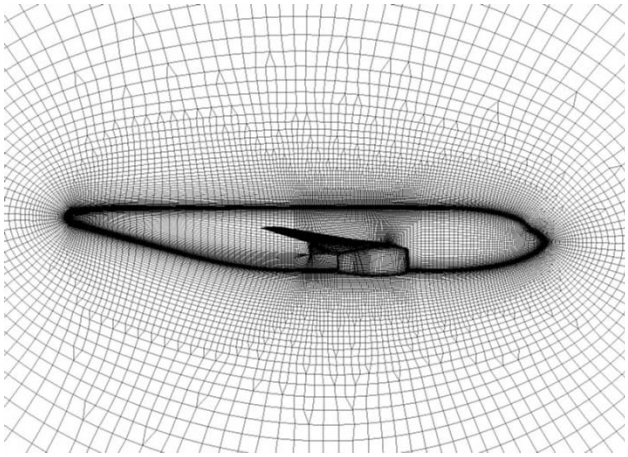

Fig. 5. Symmetry plane and surface mesh (Medium).

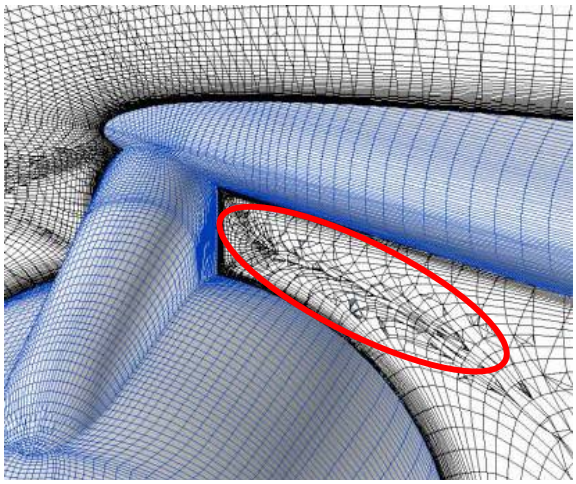

Fig. 6. An example of grid merging (concave region).

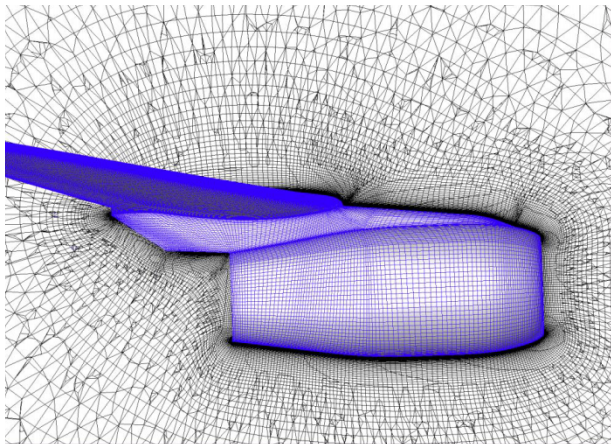

Fig. 7. Y-constant grid cross-section at center of pylon (Medium).

3 Numerical Method

In this study, the governing equations are the thin layer approximated Navier-Stokes for viscous analysis. UG3 [3] is used for flow analysis. It is a flow solver for Euler and Navier-Stokes calculations developed by authors. UG3 is based on unstructured FVM (Finite Volume Method). Spatial discretization is made by MUSCL (Monotone Upwind Scheme for Conservation Laws). SHUS (Simple High-resolution Upwind Scheme) [4] is used to calculate the approximate Riemann fluxes. Time integration is performed by MFGS (Matrix Free Gauss-Seidel method). Several turbulence models are implemented. Spalart-Allmaras one equation turbulence model [5] and Baldwin-Barth one equation model [6] are used in this study.

UG3 is parallelized using the domain decomposition method and Parallel Virtual Machine (PVM) as a message-passing library. Thus UG3 has a good scalability for a wide range of problem size. UG3 can be run on various platform such as PC, PC cluster, UNIX Workstation, UNIX SMP cluster, vector super computer, parallel super computer. PC cluster was mainly used in this study.

Table 1. Grid variations

	Grid size ;chord(*1) x span	Surface cells	Volume nodes	Volume cells	Comment
Wing/Body	Coarse; 104 x 67	22k	1.6M	1.8M	span(--)
	Coarse-mod; 104x93	44k	2.8M	3.2M	span(-)
	Medium; 104 x 121	57k	3.6M	4.1M	nominal
	Fine; 204 x 88	73k	4.7M	5.2M	chord(+)
	Fine-mod; 104 x 121 (*2)	57k	6.3M	7.5M	normal(+)
Wing/Body/ Nacelle/Pylon	Coarse; 104 x 84	49k	2.8M	3.3M	sapn(-)
	Medium; 104 x 163	105k	5.9M	6.7M	nominal
	Fine; 204 x 163	160k	8.6M	9.5M	chord(+)

*1 on single side wing surface
*2 normal direction grid points were increased (120 -> 204)

Table 2. Computed cases (Re=3x10^6,Mach=0.75. α=0.49 for WB, CL=0.5 for WBNP)

Case Name	Grid	Turb. model	Transition	WB	WBNP
Nominal	Medium	Spalart-Allmaras	Fully turbulent	√	√
Grid sensitivety analysis	Coarse	Spalart-Allmaras	Fully turbulent	√	√
	Coarse-mod	Spalart-Allmaras	Fully turbulent	√	–
	Fine	Spalart-Allmaras	Fully turbulent	√	√
	Fine-mod	Spalart-Allmaras	Fully turbulent	√	–
Turbulaence model	Medium	Baldwin-Barth	Fully turbulent	√	√
Transition	Medium	Spalart-Allmaras	Tripped (*3)	√	√
Turb. and Transition	Medium	Baldwin-Barth	Tripped (*3)	√	√

*1 on single side wing surface
*2 surface mesh is the same as Medium grid
*3 Trip location was approximately adjusted with wind tunnel test result

Table 3. Computed cases for Angle of attack sweep.

Grid	Turb. Model	Transition	Alpha sweep
Medium	Spalart-Allmaras	Fully turb.	2 points
Medium	Spalart-Allmaras	triped	full
Medium	Baldwin-Barth	Fully turb.	2 points
Medium	Baldwin-Barth	triped	full

4 Computed Cases

Computed cases are summarized in Tables 2 and 3. Grid density, turbulence modeling, and transition sensitivity analysis were conducted. Angle of attack (α) sweep was conducted as shown in Table 3 to compare polar curve and three components of force with wind tunnel test data. All computations in this paper were done at Reynolds number = 3x10^6, Mach number = 0.75.

For the grid density sensitivity analysis, we computed both α matched condition and CL matched condition. α matched condition means angle of attack is fixed in spite of difference in CL value. CL match condition means CL was adjusted to the same value 0.5 by modifying α. The α matched condition is suitable to compare particular aerodynamic characteristics such as pressure distributions and separation between various grids, while the CL matched condition suits to compare total forces.

The total amount of computed cases is more than 40. Calculation CPU time is half day using 8 CPU PC cluster for typical WB case.

5 Results and discussion

5.1 Wing/Body Configuration

Grid density sensitivity analysis results are shown in Fig. 8-10. These plots show pressure coefficient (Cp) distributions on the wing surface at η=0.377 span station. All these cases are α matched computations. α was fixed to 0.49.

Figure 8 indicates an effect of span direction grid density on pressure distribution. Coarse grid (number of chord direction grid points is 67), Coarse-mod grid (93), and Medium grids (121) are used. Shock location moves forward with increase of span-wise direction grid points. Because of difference in shock location, lift force is considerably changed. Shock location shift looks like converged at Medium grid.

The effect of the grid density of chord wise direction is shown in Fig. 9. Difference between two grids is small. Shock is slightly steep in fine grid results.

Figure 10 shows normal directional grid density effect on pressure distribution. While the pressure distribution is almost same, drag component differs four counts. Because spurious drag due to numerical dissipation was reduced by increase of grid density.

Three components of force in grid density sensitivity analysis are summarized in Table 4. This table denotes, too coarse grid leads to wrong result as shown by large lift and drag at coarse grid case. Coarse grid computation could not captured separation bubble at wing root junction, while medium grid successfully captured as shown in Fig. 11. Lack of grid resolution caused this wrong result. This separation bubble was also observed in WTT.

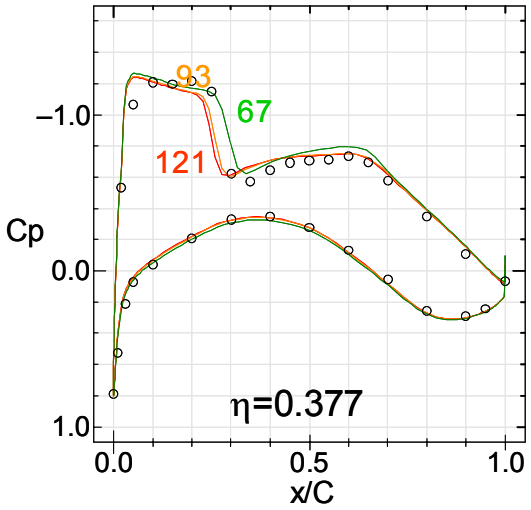

Fig. 8. Span direction grid sensitivity on Cp
67;Coarse, 93;Coarse-mod, 121;Medium grid

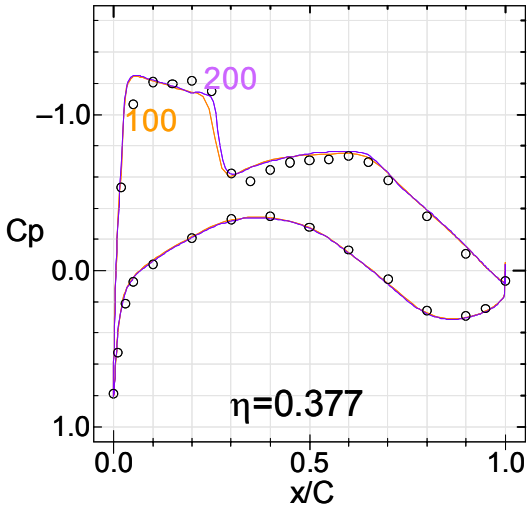

Fig. 9. Chord direction grid sensitivity on Cp
100;Medium grid, 200;Fine grid

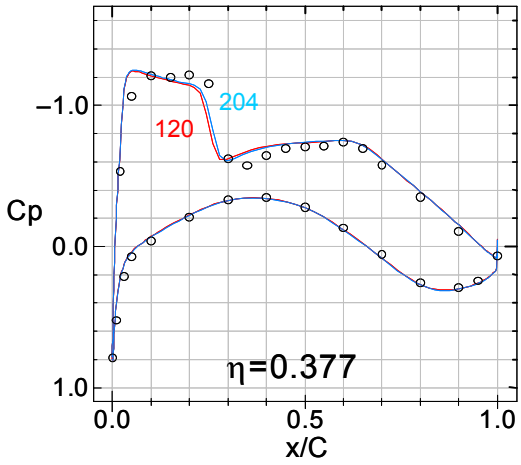

Fig. 10. Normal direction grid sensitivity on Cp.
120;Medium, 204;Fine-mod

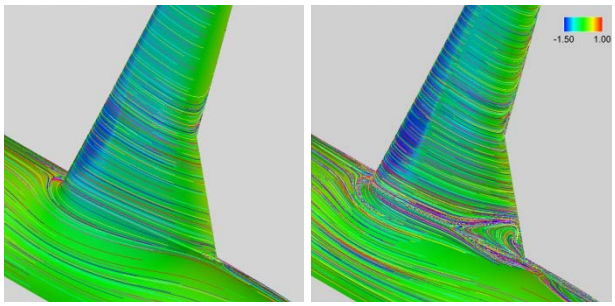

a) Coarse grid b) Medium grid

Fig. 11. Wing root separation bubble.

Two turbulence models, Spalart-Allmaras model and Baldwin-Barth model, are compared in Fig. 12. Forces of these cases are summarized in Table 5.

Spalart-Allmaras model result shows forward shock location and smaller lift and drag compared to that of Baldwin-Barth model. This disposition always appears in our computation. Take account of transition, Spalart-Allmaras model result seems to be better location. Baldwin-Barth model shows too large lift as shown in Table 5.

Figure 13 shows comparison between fully turbulent and tripped transition conditions for the Spalart-Allmaras turbulence model. Trip location was approximately adjusted to transition strips location on the wind tunnel test model. Using tripped condition, shock location moves backward, shock intensity becomes slightly strong, and surface friction drag decreases several counts.

Surface pressure distribution on Wing/Body configuration model is shown in Fig. 14. Three components of force are plotted in Fig. 15. Spalart-Allmaras (SA) turbulence model shows closer value to WTT, while Baldwin-Barth (BB) model shows large α shift. While CL-α slope computed by SA model is slightly smaller value than WTT result, CL-α slope computed by BB model is in good agreement with WTT result. Based on the Cp distribution in Fig. 12 and CM plot in Fig. 15, shock location obtained by SA model is probably precise position.

Figure 16 is a polar curve with pressure drag and surface friction drag components. Pressure drag computed by SA and BB turbulence model show very good agreement in spite of BB model has large α shift in Fig. 15. Friction drag shows constant gap between two turbulence models. Transition effects are as follows: Increase CL by approximately +0.02. Decrease CD by approx. 4 drag counts. CL-α slope is nearly the same.

Overall agreement between CFD and WTT for Wing/Body configuration is good enough for a moderate α condition calculated in this study. α shift phenomenon should be investigated in a further study.

Table 4. Grid sensitivity study results for Wing/Body Configuration (Re=3x10^6,Mach=0.75, α=0.49)

Grid Name	Num of cells	Mach	Alpha	CL	CD	CD_PR	CD_SF	CM
Coarse	1.8M	0.75	0.49	0.5765	0.03216	0.0190	0.0132	−0.1461
Coarse-mod	3.2M	0.75	0.49	0.5257	0.03067	0.0175	0.0132	−0.1341
Medium	4.1M	0.75	0.49	0.5171	0.03061	0.0175	0.0131	−0.1321
Fine	5.2M	0.75	0.49	0.5404	0.03094	0.0178	0.0131	−0.1376
Fine-mod	7.5M	0.75	0.49	0.5247	0.03022	0.0172	0.0130	−0.1345
Wind Tunnel Test		0.75	0.49	0.5000	0.02950			−0.1211

Table 5. Turbulence model and transition effect on Wing/Body Configuration. Condition is the same as Table 4

Grid	Turbulence model	Transition	Mach	Alpha	CL	CD	CD_PR	CD_SF	CM
Medium	Spalart-Allmaras	fully turb.	0.75	0.49	0.5174	0.03062	0.0175	0.0131	−0.1322
Medium	Spalart-Allmaras	tripped	0.75	0.49	0.5292	0.03018	0.0175	0.0126	−0.1371
Medium	Baldwin-Barth	fully turb.	0.75	0.49	0.5624	0.03387	0.0199	0.0140	−0.1526
Medium	Baldwin-Barth	tripped	0.75	0.49	0.5756	0.03323	0.0199	0.0133	−0.1579

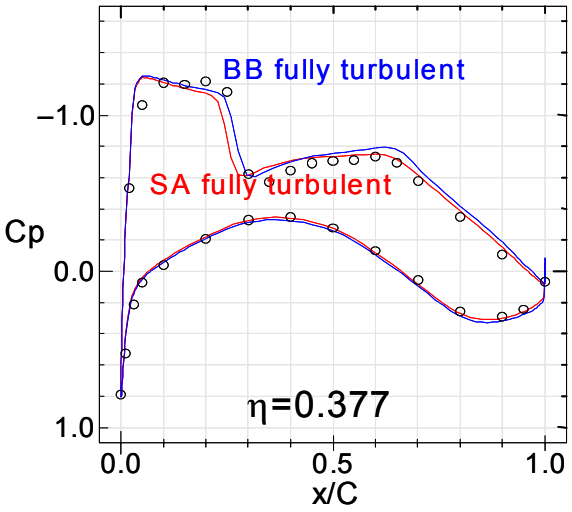

Fig. 12. Comparison between Spalart-Allmaras turbulence model (SA) and Baldwin-Barth (BB) model.

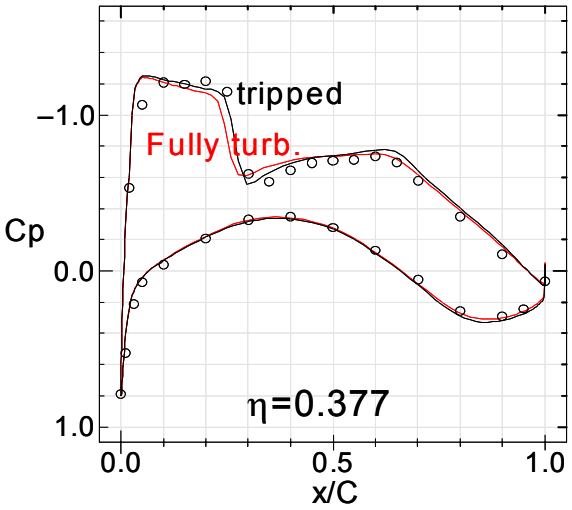

Fig. 13. Comparison between tripped and fully turbulent transition condition (SA model).

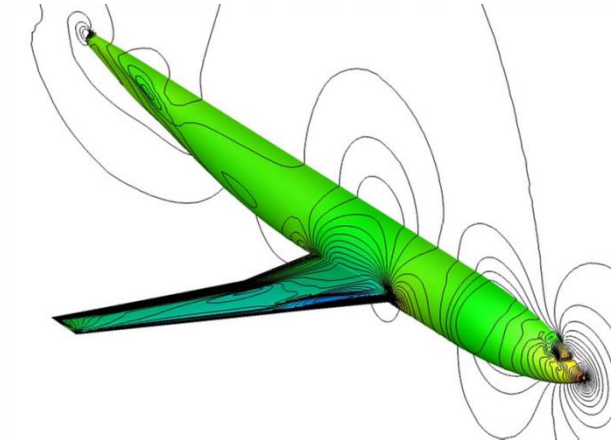

Fig. 14. Surface pressure distribution on WB. (Medium grid; Re=3M, M=0.75, α=0.5)

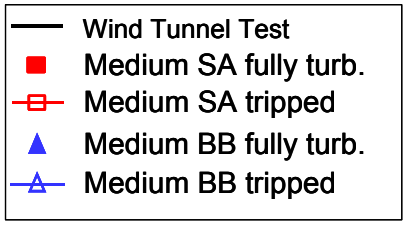

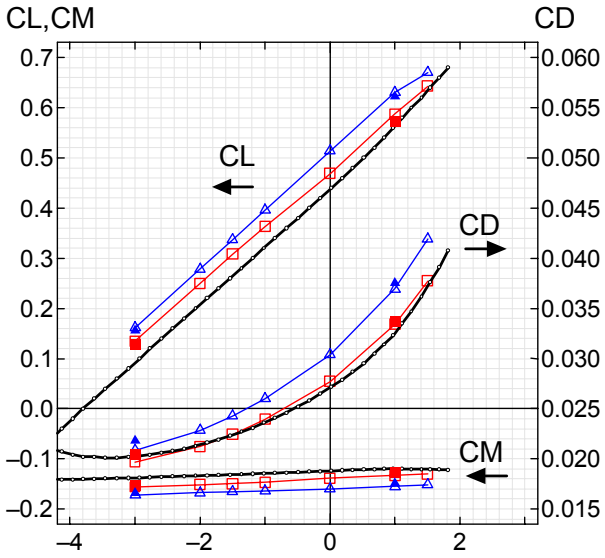

Fig. 15. Comparison of CL,CD,CM between CFD and WTT for WB configuration

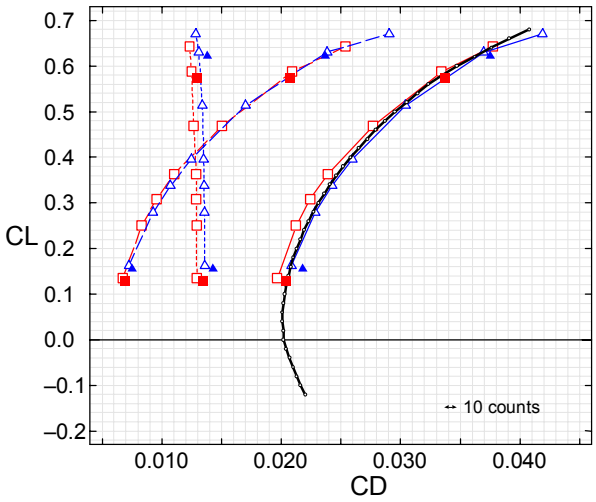

Fig. 16. Polar curve plots with pressure and friction drag component for WB configuration.

5.2 Wing/Body/Nacelle/Pylon Configuration

Surface pressure on the Wing/Body/Nacelle/Pylon (WBNP) configuration is shown in Fig. 17. Different to WB case, CL-α slope computed by SA model is considerably small compared to WTT result as shown in Fig. 18 and 19. In contrast, CL-α slope by BB model is still in good agreement with WTT. CDmin computed by CFD is larger than WTT. Drag and moment coefficient by SA is closer to WTT than BB result. Difference of polar curve between WTT and CFD is larger than Wing/Body case. Polar curve obtained by CFD is opened compared to WTT.

Pressure drag differs up to 5 drag counts around CDmin between SA and BB model. SA model shows less friction drag than BB model about 8 to 10 counts. Transition effect is just shift as same as WB configuration.

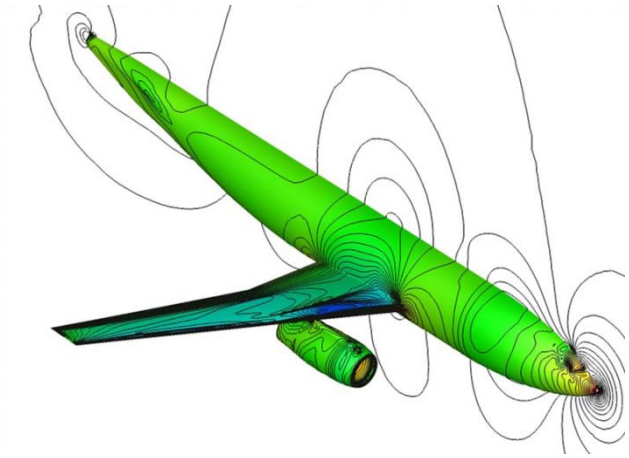

Fig. 17. Surface pressure distribution on WBNP. (Medium grid; Re=3M, M=0.75, α=1.0)

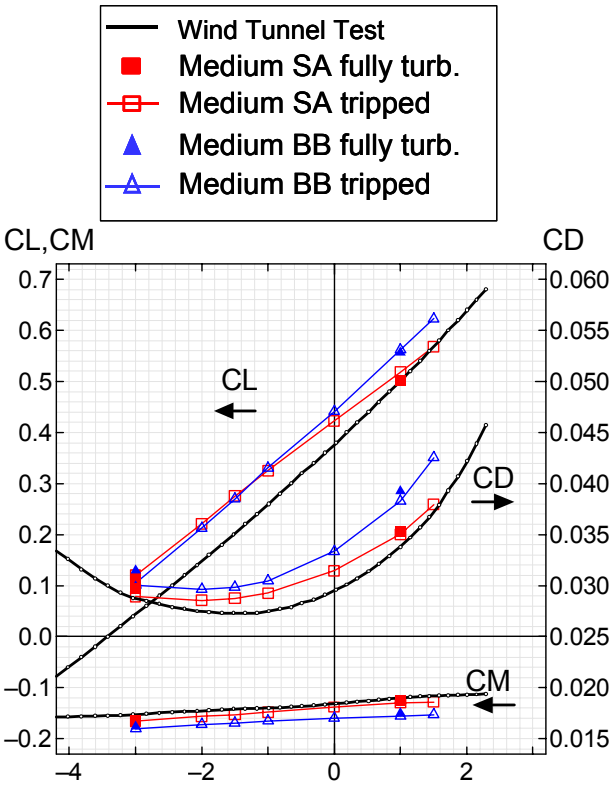

Fig. 18. Comparison of CL,CD,CM between CFD and WTT for WBNP configuration

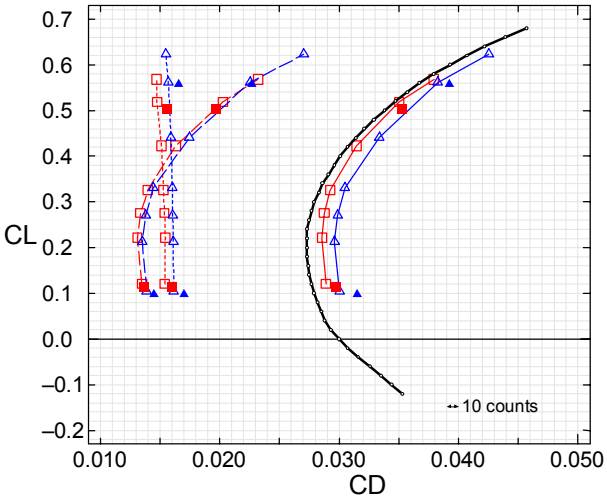

Fig. 19. Polar curve plots with pressure and friction drag component for WBNP configuration.

Table 6. Wing/Body/Nacelle/Pylon Configuration. (Re=3x10^6,Mach=0.75, CL=0.500)

GRID_SIZE		Mach	Alpha	CL	CD	CD_PR	CD_SF	CM
Coarse	3.3M	0.75	0.579	0.500	0.03390	0.01820	0.01570	−0.1391
Medium	6.7M	0.75	0.975	0.500	0.03515	0.01957	0.01588	−0.1254
Fine	9.5M	0.75	0.82	0.500	0.03460	0.01885	0.01575	−0.1294
Wind Tunnel Test		0.75	1	0.500	0.03380			−0.1199

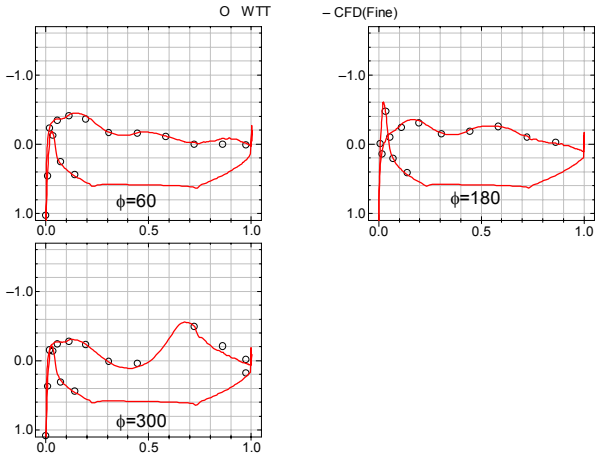

Fig. 20. Nacelle surface pressure. (Fine grid; Re=3M, M=0.75, α=1.0, SA model)

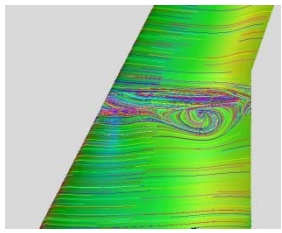

a) SA model

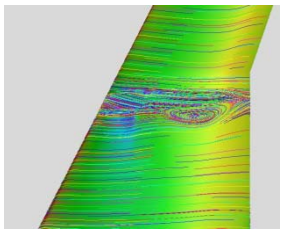

b) BB model

c) Wind Tunnel Test

Fig. 21. Oilflow visualization on lower side wing. (Medium grid; Re=3M, M=0.75, α=1.0)

Grid density sensitivity study results are shown in Table 6. These computations are CL matched calculations. Coarse grid result shows low drag because separation at wing root region was not captured as same as WB case. There is five drag counts difference between Medium and Fine grid results. It means much more grid points will be needed to obtain a grid convergence.

Figure 20 shows comparison of nacelle surface pressure between CFD and WTT. CFD is in very good agreement with WTT.

Overall agreement between CFD and WTT for Wing/Body/Nacelle/Pylon configuration is not satisfactory compared to Wing/Body cases. These inadequate results are brought by separation bubble at inboard side of pylon and wing junction. Figure 21 shows oil-flow visualization. SA model shows larger separation region than BB model result. Even BB model, separation region is larger than WTT. These separation causes discrepancy of drag component. This separation is very sensitive to grid density, turbulence model, and spatial discretization. This kind of instability loses reliability of the CFD analysis. However pressure distribution on the nacelle surface shows very good agreement. Similar to WB result, other pressure data such as wing surface was in good agreement with WTT except separated region.

6 Conclusions

Detailed survey has been conducted to validate CFD results with Wind Tunnel Test (WTT) data for Wing/Body (WB) and Wing/Body/Nacelle/pylon (WBNP) configurations. Directional grid density effect has been investigated. Overall agreement between CFD and WTT were fairly good for WB configuration. WBNP cases showed rather unsatisfactory agreement. This discrepancy was caused by sensitive separation at inboard side of pylon and wing junction. Lack of grid resolution may cause serious difference of flow separation.

Spalart-Allmaras turbulence model result was in good agreement with WTT for the WB cases, however CL-α slope was not well predicted for the WBNP configuration. On the other hand, while there are constant α shift, Baldwin-Barth model has shown stable behavior. This robustness is attractive for an aircraft design phase.

Grid convergence was not obtained through this study. Even if pressure coefficient distribution is identical, it might exist a few drag counts difference. Much more grid points will be required to get grid convergence. It awaits future studies.

References

[1] Drag Prediction Workshop Web site http://aaac.larc.nasa.gov/tsab/cfdlarc/aiaa-dpw/

[2] Ochi, A., Shima, E. A Hybrid Unstructured Grid System for Viscous and Inviscid Aerodynamic Analysis, *Proceedings of the 23rd ICAS Congress*, Paper No. 1.7.2, Sep. 2002.

[3] Shima,E., Ochi,A., Nakamura,T., Saito,S., Iwamiya,T., Unstructured Grid CFD on Numerical Wind Tunnel, in *Parallel Computational Fluid Dynamics*, pp.475-482, North Holland, (1999

[4] Shima,E. and Jounouchi,T. Role of CFD in Aeronautical Engineering (No.14) -AUSM type Upwind Schemes-", *Proceedings of the 14th NAL Symposium on Aircraft Computational Aerodynamics*, pp.7-12

[5] Spalart, P. R. and Allmaras, S. R., A One-Equation Turbulence Model for Aerodynamic Flows, *La Recherche Aerospatiale*, 1994, No.1.

[6] Baldwin, B. S., and Barth, T. J., A One-Equation Turbulence Transport Model for High Reynolds number Wall-Bounded Flows, *AIAA paper 91-0610*, 1991.

[7] Yamamoto K, Ochi A, et al., CFD Sensitivity of Drag Prediction on DLR-F6 Configuration by Structured Method and Unstructured Method, 42nd *AIAA Aerospace Sciences Meeting and Exhibit*, AIAA-2004-0398 Reno, Nevada 5 - 8 Jan 2004